Regular article

Recent advances in quantum mechanical/molecular mechanical calculations of enzyme catalysis: hydrogen tunnelling in liver alcohol dehydrogenase and inhibition of elastase by α-ketoheterocycles

Gary Tresadern, Paul F. Faulder, M. Paul Gleeson, Zubeir Tai, Grant MacKenzie, Neil A. Burton, Ian H. Hillier

Department of Chemistry, University of Manchester, Manchester, M13 9PL, UK

Abstract. Hybrid quantum mechanical (QM)/molecular mechanical (MM) calculations are used to study two aspects of enzyme catalysis, Kinetic isotope effects associated with the hydride ion transfer step in the reduction of benzyl alcohol by liver alcohol dehydrogenase are studied by employing variational transition-state theory and optimised multidimensional tunnelling. With the smaller QM region, described at the Hartree–Fock ab initio level, together with a parameterised zinc atom charge, good agreement with experiment is obtained. A comparison is made with the proton transfer in methylamine dehydrogenase. The origin of the large range in pharmacological activity shown by a series of α-keto-heterocycle inhibitors of the serine protease, elastase, is investigated by both force field and QM/MM calculations. Both models point to two different inhibition mechanisms being operative. Initial QM/MM calculations suggest that these are binding, and reaction to form a tetrahedral intermediate, the latter process occurring for only the more potent set of inhibitors.

Keywords: Liver alcohol dehydrogenase – Methylamine dehydrogenase – Quantum mechanical/molecular mechanical methods – Variational transition-state theory – Tunnelling

Introduction

The use of hybrid methods, particularly those combining quantum mechanics (QM) with molecular mechanics (MM) [1, 2, 3], to model condensed phase structure and reactivity is now well established, and has been applied to study such diverse areas as solvation, solid-state re-activity, and enzyme catalysis [4]. Although some issues such as the treatment of junction atoms, the importance of polarization of the MM region and how to properly include more than one QM level of theory, are still the subject of on-going investigation, QM/MM methods are now being used, but still not routinely, to probe the mechanism of an increasing number of enzymes [5, 6, 7, 8, 9]. These methods are now at the stage where they can be further developed and utilised to probe yet more aspects of enzyme mechanisms.

In this paper we address two such developing areas. Firstly, the study of those enzymes where reactions involving through-barrier motion, in addition to over-barrier motion, is important. The accurate treatment of such tunnelling processes requires information on the potential-energy surface (PES) in addition to the determination of the stationary structures. The second area is to see how QM/MM calculations can potentially contribute to drug discovery by leading to an understanding of the origin of the differing inhibition constants of a series of closely related molecules, where differences in binding constants alone cannot provide this insight. Both these problems present particular, and different, challenges to the QM/MM approach, which we will highlight in this paper.

Quantum mechanical tunnelling in enzyme catalysis

Hydrogen transfer, both protonic and hydridic, frequently contributes to the mechanism of enzyme-catalysed reactions and is often rate-limiting. Evidence for the importance of tunnelling in such reactions is found from the measured hydrogen kinetic isotope effects (KIEs), which may also indicate the importance of thermally induced vibrationally driven tunnelling. There is thus the need for accurate calculations of these KIEs

in order to understand the role of tunnelling in enzyme catalysis. The use of canonical variational transition-state (CVT) [10, 11] theory combined with optimised multidimensional tunnelling (OMT) [10, 11, 12, 13, 14] methods has been shown to be extremely successful in predicting both rate constants and hence KIEs for small gas-phase reactions [14], for example, those of importance in combustion processes. In view of the need to evaluate Hessians at a large number of points along the reaction pathway such calculations are extremely time consuming, and even for reactions of small molecules the strategy is usually to employ full calculations at a low level and correct these with data from a limited number of high-level calculations, such as those of the stationary points on the PES [15, 16]. Such a dual level approach is now well established as an accurate, yet computationally feasible, way of predicting rate constants. For enzymatic reactions where a large number of atoms usually participate actively in the mechanism, there are alternative ways in which PESs can be calculated and used in CVT and tunnelling treatments. In a recent study of the hydride transfer step catalysed by xylose isomerase Nicoll et al. [7] used a combined QM/MM potential, employing the semiempirical PM3 Hamiltonian, whilst in a study of hydride transfer catalysed by liver alcohol dehydrogenase (LADH), Alhambra et al. [6] employed a QM/MM potential, augmented by a semiempirical valence bond term to correct inadequacies in the hybrid AM1/CHARMM22 PES. We here explore alternative approaches for obtaining a QM/MM potential which can be combined with CVT and multidimensional tunnelling to predict the KIEs associated with hydride transfer catalysed by LADH.

The active site of LADH is shown in Fig. 1. The substrate, benzyl alcoholate, is coordinated to the Zn^{2+} ion, which also has two cysteine ligands and one histidine ligand. Hydride transfer is to carbon atom 4 of the NAD^+ cofactor. This reaction was modelled using our QM/MM code, which links Gaussian 94 [17] and AMBER [18]. In the calculations described here, the covalent junctions between the QM and the MM regions were treated using the link-atom method [3]. Structural data were prepared from the experimental crystal coordinates of horse LADH (EC: 1.1.1.1) [19], in which the Trp93 residue was mutated to Phe93 as in the native enzyme. The nonstandard residue, benzyl alcoholate, was then added to the crystal structure along with the coenzyme, NAD^+. The entire MM structure was protonated and then minimised with the AMBER MM force field [20] using the parameters of Ryde [21]. The minimised structure showed good agreement with the crystal structure, especially concerning the heavy-atom arrangement within the proton relay system (NAD^+–ribose– His51– Ser48– substrate) and the coordination around the zinc ion. This structure was then used in two QM/MM calculations which differed in the size of the QM region. In the calculation (C1) with the larger QM region, 54 atoms (Fig. 2), the AM1 semiempirical Hamiltonian was employed for the QM region. A cal-
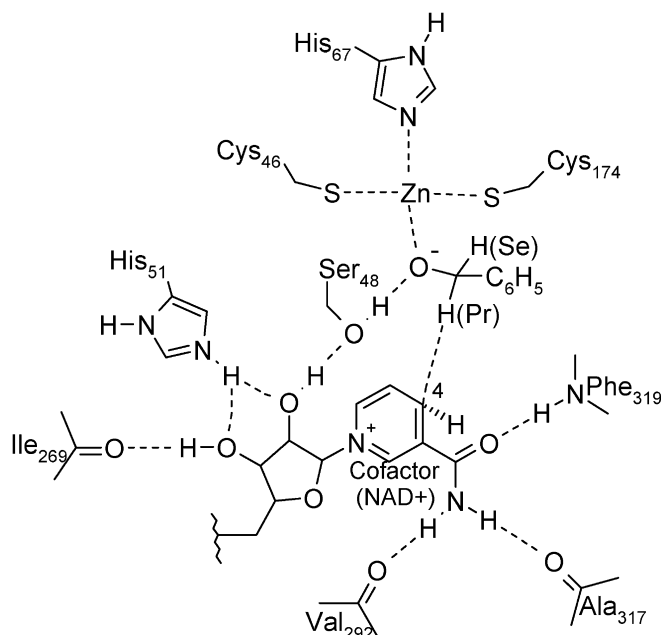

Fig. 1. Liver alcohol dehydrogenase (*LADH*) active site, with primary (*Pr*) and secondary (*Se*) hydrogens labelled
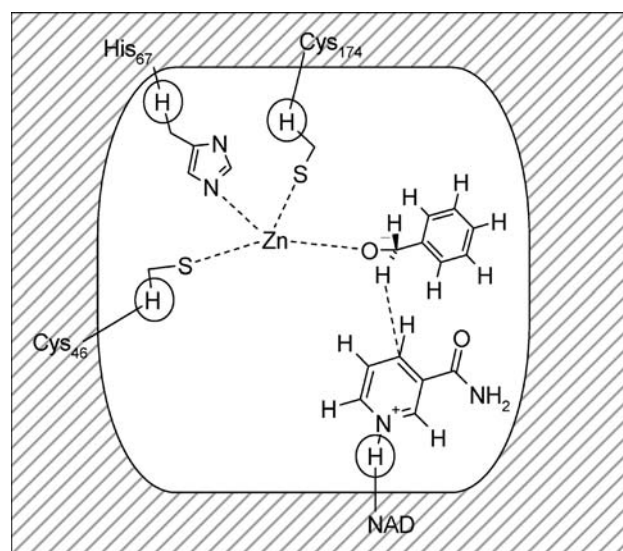

Fig. 2. LADH quantum mechanics (*QM*)/molecular mechanics (*MM*) region for model 1 (C1); link atoms are *circled*

culation having a smaller QM region (44 atoms, Fig. 3) was also employed (C2), which allowed ab initio Hartree–Fock calculations to be performed to locate the stationary structures on the PES. In this calculation (C2) the zinc ion was included in the MM region, but owing to the sensitivity of the PES to the formal metal charge, this quantity was treated as an adjustable parameter.

The direct dynamics calculations were carried out for both QM/MM models. We use our adaption of GAUSSRATE [22] to link the POLYRATE package of Truhlar and others with our QM/MM code. Both
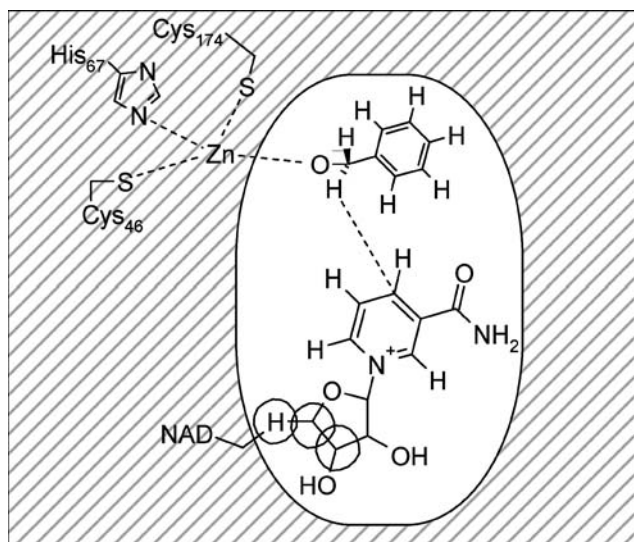
Fig. 3. LADH QM/MM region for model 2 (C2); *circled* atoms were fixed

QM/MM models were treated, the reaction paths being calculated with the AM1 Hamiltonian and using the Page and McIver algorithm [23]. For the larger QM system (C1), the calculation of the reaction path was limited owing to computational expense. The reaction path was calculated with a step size of 0.01 amu$^{1/2}$ bohr with Hessians calculated every second step and gradients at every step. The reaction path was calculated to limits of −0.6 and 0.4 amu$^{1/2}$ bohr, and then interpolation was performed to −2.4 and 1.0 amu$^{1/2}$ bohr. The transmission coefficients were evaluated using the zero-curvature (ZCT) [11], small-curvature (SCT) [12, 24] and large-curvature tunnelling [25] methods, the largest value being used in the OMT calculations. The ZCT and SCT methods calculate tunnelling through the adiabatic potential-energy curve. However, the two models differ by the use of an effective reduced mass in the SCT case as opposed to a more simple reduced mass for ZCT. The effective reduced mass is decreased as the reaction path curvature increases. Regions of reaction path curvature arise when the motion along the reaction coordinate is coupled to any transverse vibration. For a given reaction pathway with more curvature the contribution to tunnelling would be expected to increase owing to corner cutting by the transferring particle.

With the ab initio stationary structures for the smaller QM/MM model, C2, it was possible to perform a dual level calculation, using variational transition-state theory (VTST) with interpolated optimised corrections (IOC) [15, 16]. The VTST– IOC method used here incorporates information from stationary points that have been found at a higher level than that used for the calculation of the reaction pathway. In particular, the energies, frequencies and moments of inertia at the lower-level stationary points are all directly corrected and then an interpolated correction is applied to all nonstationary points along the reaction path. The AM1 potential was interpolated using a single Eckart potential fit to the differences between the lower- and higher-level energies The frequencies were corrected using the interpolated corrections based on logarithms method [15, 16].

We have calculated both primary and secondary KIEs for deuterium and tritium substitution, for both QM/MM models. Swain–Schaad exponents [26, 27, 28],

$$\alpha = \frac{\ln(k_\mathrm{H}/k_\mathrm{T})}{\ln(k_\mathrm{D}/k_\mathrm{T})} , \qquad (1)$$

have also been calculated for both primary and secondary isotopic substitution. A value greater than 3.3 has been found experimentally [29] and is believed to be symptomatic of tunnelling. We use the notation $\left(k\,{}^\mathrm{Se}_\mathrm{Pr}\right)$ to identify the isotope at the primary (Pr) and secondary (Se) positions, as shown in Fig. 1. Rate constants and transmission coefficients were calculated at 300 K, the transmission coefficients being calculated by the OMT method, using the SCT approximation.

We first discuss the model with the larger QM region (C1), the reaction profile for no isotopic substitution being shown in Fig. 4. The potential-energy barrier (Fig. 4, line a, V_MEP), 8.2 kcal mol^{-1}, was reduced to 6.1 kcal mol^{-1} with the inclusion of zero-point-energy (ZPE) effects (Fig. 4, line b, V_a^G), a value significantly less than the experimental activation energy of 15.6 kcal mol^{-1} [30].

The variational effect is noticeable when the potential and adiabatic energy curves are compared, indicating that recrossing effects are significant and that the inclusion of ZPE has produced an earlier transition state with a shorter breaking C–H bond. The variational transition state moves from −0.22 to −0.08 amu$^{1/2}$ bohr upon primary tritium substitution. This variational effect arises from the comparatively late change in the ZPE as the reaction proceeds from reactant towards transition state.

The KIEs are presented in Table 1. The primary KIEs for the larger QM system, C1, are smaller than the experimental values for all levels of theory, the TST results being closer to experiment than are the CVT ones, which show an unexpectedly large reduction as a consequence of the substantial variational effect on k_H^H compared to k_T^H. The variational transition state is earlier along the reaction path for k_H^H −0.22 versus −0.08 amu$^{1/2}$ bohr, and as a consequence there is a greater difference between the TST and CVT rate constants, k_H^H, than for k_T^H. At 300 K the corresponding values are k_H^H (TST) = 1.13 × 10^8 s^{-1} and k_H^H (CVT) = 8.10 × 10^7 s^{-1}, compared to k_T^H (TST) = 2.42 × 10^7 s^{-1} and k_T^H (CVT) = 2.33 × 10^7 s^{-1}. Inclusion of tunnelling improves the CVT KIE, increasing it from 3.48 to 3.93, owing to differences in the transmission coefficients $\kappa_\mathrm{H}^\mathrm{H}$ and $\kappa_\mathrm{T}^\mathrm{H}$, 1.88 and 1.65, respectively.

The secondary KIEs show better agreement with experiment, and again the agreement is improved by the inclusion of tunnelling. The calculated Swain–Schaad exponents reflect the errors present in the KIEs. The
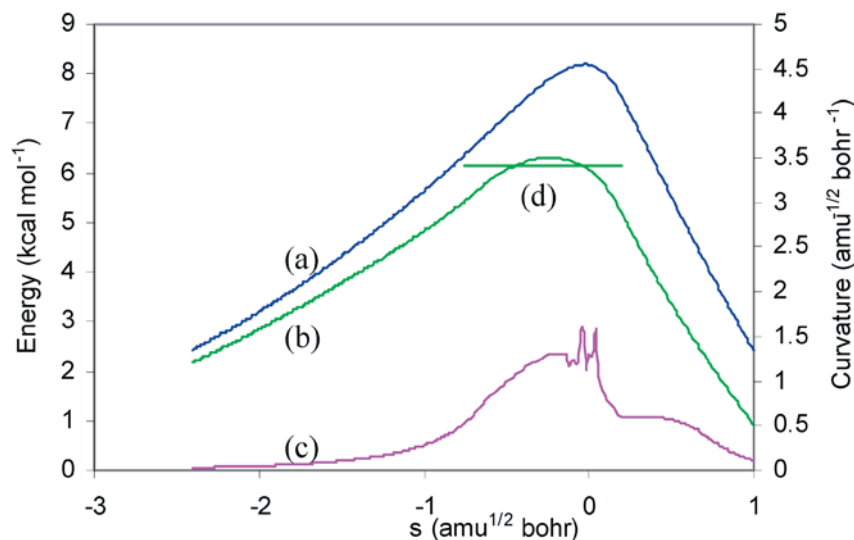
Fig. 4. LADH hydride transfer, AM1 energetics (*left scale*) and total reaction path curvature (*right scale*) for a 54-atom system (C1). *a* Potential energy, V_{MEP}, relative to reactant. *b* Vibrationally adiabatic potential energy, V_a^G, relative to reactant. *c* Total reaction path curvature. *d* The *horizontal line* is the representative tunnelling energy (*RTE*) through V_a^G

Table 1. Primary and secondary kinetic isotope effects (*KIEs*), and Swain–Schaad exponents for hydride transfer in 54-atom and 44-atom quantum mechanics (*QM*)/molecular mechanics (*MM*) liver alcohol dehydrogenase models. Exponents calculated from unrounded KIEs. AM1 single-level results on large QM/MM system (C1). The results in *parentheses* are for HF/3-21G///AM1 calculations on a smaller model (C2). The experimental results are those of of Bahnson et al. [29]

	TST	CVT	CVT/OMT	Experiment
		Primary KIE		
k_H^H/k_T^H	4.67 (6.32)	3.48 (5.18)	3.93 (7.27)	7.1
k_D^D/k_T^D	1.60 (1.74)	1.53 (1.69)	1.58 (1.89)	1.9
		Secondary KIE		
k_H^H/k_H^T	1.12 (1.26)	1.18 (1.30)	1.25 (1.70)	1.33
k_D^D/k_D^T	1.03 (1.07)	1.03 (1.07)	1.06 (1.14)	1.07
		Exponents		
α_{prim}	3.29 (3.35)	2.95 (3.15)	3.02 (3.11)	3.1
α_{sec}	3.55 (3.23)	4.79 (3.72)	3.95 (4.08)	4.1

primary exponent is too small at the CVT level but is improved slightly with the inclusion of tunnelling. The values of the secondary exponents are more varied, and the CVT result is much too large, but the inclusion of tunnelling gives the best agreement with experiment. Clearly, there are inadequacies in the use of an uncorrected QM(AM1)/MM potential. We now consider a model designed to address this problem.

A smaller QM system of 44 atoms was chosen that would allow us to perform ab initio calculations of the stationary points on the PES to be subsequently used in a dual level direct dynamics calculation of reaction rates. For the 44-atom system the zinc atom was placed in the MM region, and QM/MM calculations were performed at the HF/3-21G level [31]. Reactant, transition state and product stationary points were found for a range of zinc charges using the coordinate driving approach. The results are summarized in Table 2. The large effects of varying the formal zinc charge on both the barrier height and shape are evident. An increase in the charge clearly preferentially stabilizes the reactant, thereby increasing the barrier height and reducing the exothermicity of the

reaction. In the actual enzyme the ligands bound to the zinc ion can effect such a modulation of the atomic charge. Within our QM/MM model, we can choose the effective zinc charge to best reproduce the experimental energetics. With a charge of 1.15 *e* the barrier for the reaction was 18.6 kcal mol^{-1}, being reduced to 15.2 kcal mol^{-1} upon the inclusion of ZPE, which compares favourably to the experimental value of 15.6 kcal mol^{-1}. This ab initio calculation was then used in a dual level calculation of the rate constants, which employed the AM1 Hamiltonian for the lower level part of the calculation. At the AM1 level and with the same zinc atomic charge (1.15 *e*) the barrier for reaction was only 7.3 kcal mol^{-1} reducing to 5.0 kcal mol^{-1} with the inclusion of ZPE. The calculated activation energy at the AM1 level will thus be considerably lower than the experimental value (15.6 kcal mol^{-1}), requiring the use of the dual level approach. The imaginary frequency of the transition state was 799 *i* cm^{-1} (AM1), which was corrected in the dual level calculation to 1,229 *i* cm^{-1} from the HF/3-21G results. The dual level direct dynamics calculations were performed with a step size of 0.01 amu$^{1/2}$ bohr with Hessians evaluated every

Table 2. Barrier heights, energies of reaction(kcal mol^{-1}) and imaginary frequencies (cm^{-1}) calculated at the HF/3-21G level with the corresponding zinc atom MM charge (e)

Zinc MM charge	Barrier height	Reaction energy	$\bar{v}_i$
0.488 [a]	7.16	−38.09	820 i
1.0	14.24	−17.57	1,139 i
1.15	18.60	−8.06	1,229 i
1.50	42.42	32.82	1,042 i

[a]The charge found by Ryde [21]

second step and gradients at all points in between. The reaction path itself was then calculated to limits of ± 1.5 amu$^{1/2}$ bohr, at which point the transmission probabilities for tunnelling trajectories for the k_H^H process were less than 10^{-6}. The calculated V_{MEP} and V_a^G PESs and the total reaction path curvature for k_H^H are shown in Fig. 5. It is immediately clear that there is still a large variational effect on V_a^G. The variational transition state moves from −0.15 to −0.03 amu$^{1/2}$ bohr upon primary tritium substitution. This is pleasing as it means that our smaller QM/MM model (C2) is still exhibiting the same features of the large one (C1). Furthermore, from calculating a larger reaction path we can identify a second peak in the reaction path curvature on the product side, which is typical for hydrogen transfer reactions of this type (Fig. 5, line c). As a result of the increase in reaction path curvature and the much larger barrier, we observe increased amounts of tunnelling for model C2. At 300 K, κ_H^H and κ_T^H were calculated to be 3.22 and 2.29, respectively.

The representative tunnelling energy (RTE) [13, 32], is the energy at which tunnelling is most likely to occur for a particular temperature, and has been calculated for both models. This quantity is defined as being the energy at which the integrand of the numerator of the ground-state transmission coefficient ($\kappa^{CVT/G}(T)$, Eq. 2 [11]) is a maximum.

$$\kappa^{CVT/G}(T) = \frac{\int_0^\infty P^G(E) \exp(-E/k_B T)dE}{\int_0^\infty P_C^{CVT/G}(E) \exp(-E/k_B T)dE} \quad (2)$$
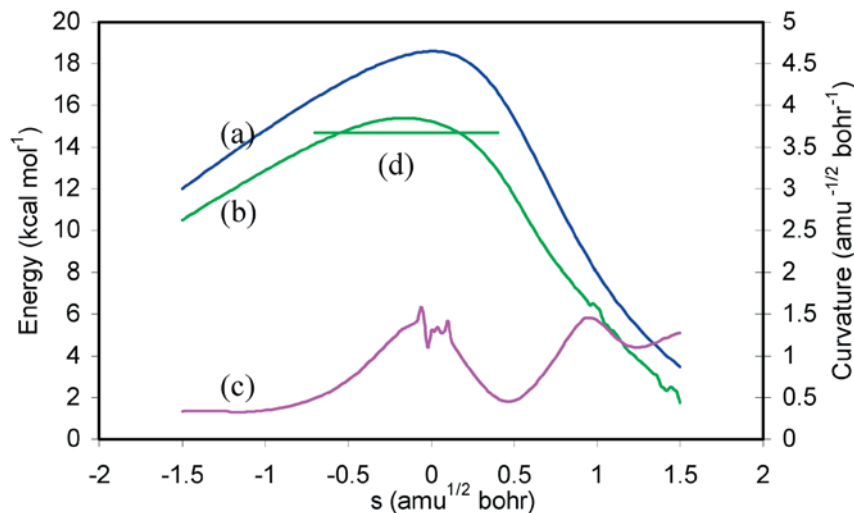
Here $P^G(E)$ is the thermally averaged quantal transmission probability, $P_C^{CVT/G}$ is the thermally averaged classical transmission probability, which is zero below $V_a^G(s = s_*^{CVT})$, and unity otherwise. There is competition between the Boltzmann factor, which decreases with energy, and the tunnelling probability, which increases with energy [13]. There are two points on the reaction path where the RTE equals the adiabatic energy. The straight line between these two points is termed the representative tunnelling path. For LADH the dominant tunnelling energy was 0.7 kcal mol^{-1} below the top of the barrier, (C2, Fig. 5, line d), and the entrance and exit tunnelling geometries occurred either side of the first region of reaction path curvature (Fig. 5, line c).

With the inclusion of tunnelling by multidimensional methods we find excellent agreement for the primary KIEs, $k_H^H/k_T^H = 7.27$ and $k_D^D/k_T^D = 1.89$ (Table 1) compared to the experimental values of 7.1 and 1.9, respectively. Although the secondary KIEs do not correlate as well with experiment, the Swain–Schaad exponents do show good agreement with experiment. With the inclusion of tunnelling the agreement is again excellent, 3.11 and 4.08 calculated compared to 3.1 and 4.1 from experiment.

From our study of LADH we can conclude that the increase in the secondary Swain–Schaad exponent does arise from tunnelling. Only with the inclusion of corner-cutting effects was the best agreement found, as the ZCT method underestimated the amount of tunnelling and

Fig. 5. LADH hydride transfer, HF/3-21G/// AM1 energetics (*left scale*) and total reaction path curvature (*right scale*) for a 44-atom system (C2). *a* Potential energy, V_{MEP}, relative to reactant. *b* Vibrationally adiabatic potential energy, V_a^G, relative to reactant. *c* Total reaction path curvature. *d* The *horizontal line* is the RTE through V_a^G

did not produce Swain–Schaad exponents in agreement with experiment. Excellent agreement was found with the inclusion of tunnelling, especially for the primary KIEs. Using a more accurate vibrationally adiabatic potential-energy barrier produced the best results. However, the smaller barrier was successful in predicting many of the reaction's characteristics, such as similar magnitudes for the reaction path curvature before the transition state, and moderate amounts of tunnelling.

We have reported preliminary calculations of the KIEs associated with proton transfer in methylamine dehydrogenase (MADH) [9], where, in contrast to LADH, large primary deuterium KIEs are observed (11.1 calculated at 300 K compared to 16.8 from experiment [33]). The differences can be understood by comparing the reaction paths for the two enzymes which we have calculated. V_a^G and the reaction path curvature for LADH and MADH are compared in Fig. 6, and the differences are striking. For MADH the adiabatic potential is much narrower, which is symptomatic of less heavy atom movement along the reaction pathway, producing significantly more tunnelling. Corner-cutting tunnelling was found to be important for LADH and was influenced by the regions of reaction path curvature before and after the transition state. However, for MADH the curvature maxima (Fig. 6, line d) are considerably larger as a result of increased coupling of the vibrations of the breaking and forming bonds to the reaction pathway. Consequently the mechanism of corner-cutting tunnelling is even more important. The RTE for MADH at 300 K is 3.7 kcal mol^{-1} below the top of the barrier compared to 0.7 kcal mol^{-1} for LADH, which again demonstrates the increased tunnelling in MADH.

In summary, for both LADH and MADH we observe a quantum mechanical tunnelling contribution to the enzymatic mechanism. However, for MADH this is significantly larger as a consequence of the lack of heavy atom movement along the reaction pathway, and the increased coupling of the vibrational modes to the reaction path which creates a pathway with greater curvature. The vibrational modes of MADH are more susceptible to coupling with the reaction pathway because the C–H bond is broken both earlier and over a shorter distance, whereas for LADH there is more structural rearrangement required prior to hydride transfer and a gradual breaking of the C–H bond.

Inhibition of elastase by peptidyl α-ketoheterocyclic compounds

Modelling studies based upon empirical force fields of varying degrees of sophistication are commonly used to understand the origin of pharmacological activity as reflected in measured potency, traditionally reported as K_i values. Such values of K_i are expected to depend on the free energy of substrate–enzyme binding which requires the free-energy change accompanying the substrate transferring from an aqueous environment to the enzyme binding site. Methods used to carry out such simulations traditionally include free-energy perturbation studies [34], empirical linear response methods [35] and scoring functions [36], and with suitable parameterisation all have been quite successful. Naturally such models only include noncovalent interactions and do not include the potential for a chemical reaction occurring at the enzyme active site, which can best be modelled with QM/MM methods.
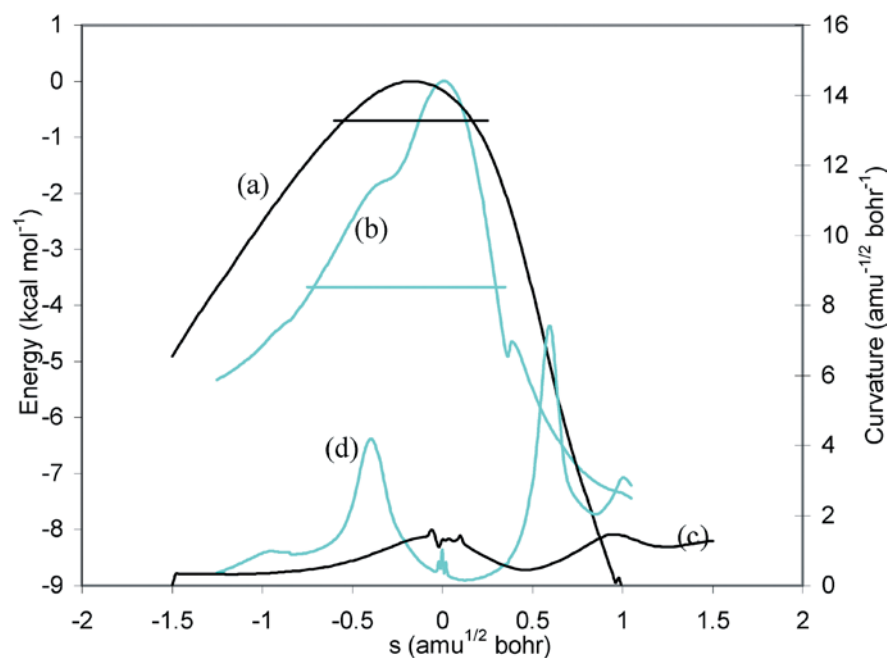
Fig. 6. Comparison of hydride transfer in LADH, HF/3-21G///AM1 and proton transfer in methylamine dehydrogenase (*MADH*), PM3 level. Relative energetics (*left scale*) and total reaction path curvature (*right scale*). *a* V_a^G for hydride transfer in LADH. *b* V_a^G for proton transfer in MADH. *c* LADH hydride transfer total reaction path curvature. *d* MADH proton transfer total reaction path curvature. The *horizontal lines* are the RTEs through V_a^G

The serine proteases are a class of enzyme much studied experimentally, but in spite of their importance few computational studies have been reported. A series of peptidyl α-ketoheterocyclic inhibitors of the serine protease, elastase, have been studied experimentally [37] and show a wide range of K_i values, associated with quite subtle changes in molecular structure. The general mode of binding of such a ketonic inhibitor or a natural peptide substrate at the elastase active site [38], consisting of the catalytic triad (His57, Ser195 and Asp102), and oxyanion hole (Gly193 and Ser195), is shown in Fig. 7, illustrated with the former substrate.

Whereas cleavage of the amide C–N bond can occur in the natural substrate, following nucleophilic attack by Ser195, in the case of the ketonic inhibitors such attack leads to the formation of a tetrahedral intermediate which cannot react further. It has been suggested that the more potent ketonic inhibitors (K_i below 1,000 nM) may undergo chemical reaction at the active site to form such a tetrahedral intermediate, whilst the less potent molecules (K_i above 1,000 nM) may inhibit by noncovalent interactions to yield the Michaelis complex [37]. Although the evidence for this is not conclusive, relying on a correlation of the experimental activity with the Hammett σ values [39] of the terminal unsaturated ring of each inhibitor, the analysis did suggest a difference between the two sets of inhibitors. Another study [40], again using a quantitive structure activity relationship (QSAR) approach, found that both the LUMO of the ketone and the charge of the heteroatom in the unsaturated ring correlated with the K_i values for the more potent set. However, the study did not answer the question of whether there are two distinct modes of inhibition. It is clear that more detailed modelling studies are needed to gain further insight into the binding and possible reactivity of these substrates.
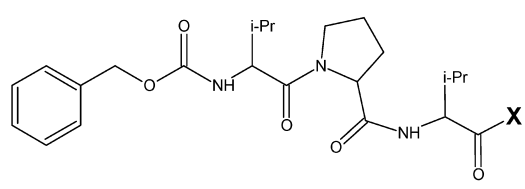
We herein report preliminary studies of the binding of a representative number of peptidyl α-ketoherocyclic inhibitors, shown in Table 3 chosen to span the large range of K_i values observed experimentally and differing solely in the nature of the terminal unsaturated ring (X).
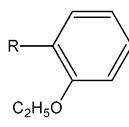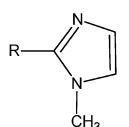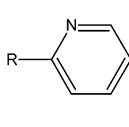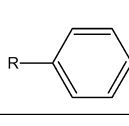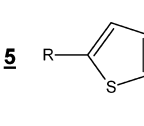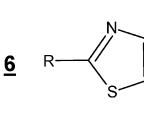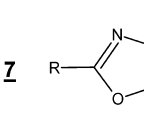
No crystal structure showing the binding of such ketonic inhibitors is available; however the structure of a Michaelis complex of elastase with a natural peptide inhibitor (1PPF, 1.8 Å) [41], having the requisite substrate–active site interactions was used to generate initial models of the ketonic inhibitors bound at the active site. The substrate was approximated by X – Val– Pro– CH_3 to ensure proper binding within the elastase active site. Apart from the primary interactions with the triad and oxy-anion hole, the interaction with Phe41 is crucial for the correct orientation of natural substrates within the active site [41]. Standard AMBER [18] force field parameters [20] were used to describe the enzyme and, where possible, parts of the substrate. For those parts of the substrates consisting of nonstandard residues, appropriate parameters were chosen to ensure that the terminal unsaturated rings remained planar with the adjacent carbonyl group, and had barriers to rotation in line with those calculated from Hartree–Fock 6-31G* [31] calculations. Formal electrostatic potential atomic charges [42] for the seven substrates modelled (Table 3) were also obtained at this level of theory, in line with the standard AMBER charges used. An initial structure was generated by replacing the natural substrate (Fig. 8a) in 1PPF with the inhibitor having a terminal phenyl group (Fig. 8b), followed by solvation with a box of water consisting of about 4,500 water TIP3P molecules.

A problem with the initial unoptimised structure arose because the direction of the amino acid sequence in the natural substrate is opposite to that in the inhibitors, resulting in a less than adequate binding conformation, specifically the lack of interaction with Phe41. However, on the basis of the geometrical requirements for the interaction of the inhibitor carbonyl group with the oxyanion hole and with the serine nucleophile, as well as the interaction of the inhibitor heterocycle with His57, it was a straightforward procedure to dock the inhibitor. This structure was optimised in AMBER4.1 [18] using periodic boundary conditions to a root mean square of approximately 1×10^{-2} kcal mol^{-1} followed by equilibration employing 400 ps of molecular dynamics simulation to improve the position of the substrate
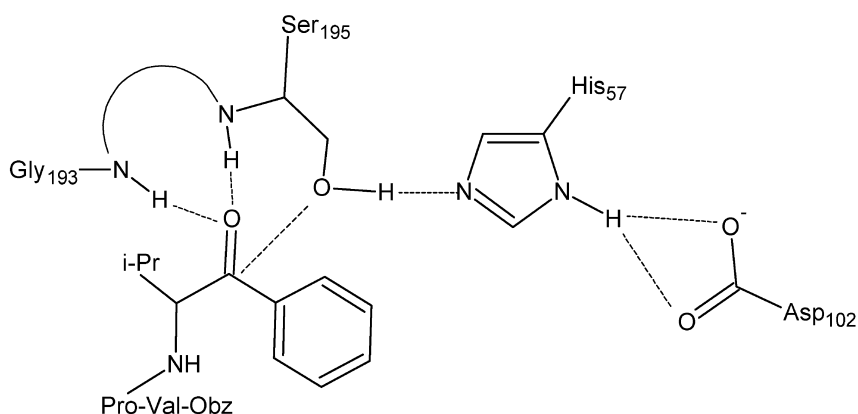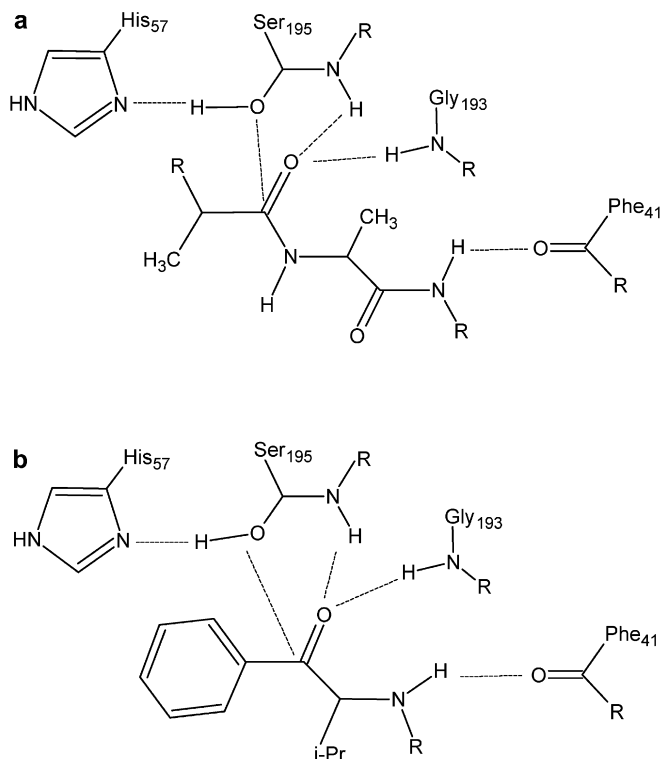

Fig. 7. A peptidyl α-ketoheterocyclic compound bound to a typical serine protease active site

Table 3. A range of peptidyl α-ketoheterocyclic compounds and their K_i values

Inhibitor Number - Heterocycle (X) - K_i(nM)

Fig. 8. a A typical peptide bound at the elastase active site. **b** An α-ketoheterocyclic inhibitor (4) bound at the elastase active site

within the active site and the provision of a more accurate enzyme structure. This involved heating the system to 300 K (100 ps), equilibration (150 ps) and cooling to 0 K (150 ps), followed by optimization of the final structure. This simulation was successful in improving the position of the substrate within the active site, evident by the formation of a strong interaction with Phe41. The new active-site configuration had all the necessary interactions for this inhibitor and was therefore used as a template for generating the initial structures of the other inhibitors, which differed only in the type of terminal ring. For the six other substrates both possible planar orientations of the unsaturated ring were considered. All such structures were solvated and equilibrated as before. Appropriate models of the solvated substrates were generated using the initial conformations of the substrate, identical to that found in each Michaelis complex, which were solvated in a box of water consisting of about 400 TIP3P water molecules and again were energy-minimised to a root mean square less than 1×10^{-2} kcal mol^{-1}.

We are interested in the relative rather than the absolute binding energies of the different substrates in the enzyme active site, which can be taken to be given by the difference in interaction energies of the substrate in the two environments, enzyme and aqueous solution. As a result of the considerable homology between the

different inhibitors, and assuming they bind in an identical manner, the variation in activity should arise solely owing to the difference in structure of the unsaturated rings [37]. This led us to conclude that, as an approximation, the entropic term can be neglected and the relative binding energy can be explained by enthalpy differences only. A purely MM interaction energy, consisting of the van der Waals and the electrostatic interactions, was calculated between the substrate and its two environments, enzyme and the aqueous solution. For each substrate, the conformation affording the greatest interaction with the surroundings was used to calculate the relative binding energy and was plotted against $\ln K_i$, the results being given in Fig. 9. When one considers the small data set used and the single descriptor employed (binding energy) the r^2 value of 0.53 is quite acceptable.

These results show that the substrates interact better with the enzyme environment than with the solvent, although this force field treatment does not take into account any contribution of conformational change of the substrate to the binding energy. It is clear however that the substrates do indeed fall into two classes. For the less potent set (1–5) there is a good correlation between the relative binding energies and experimental activities, whilst for the more potent set (6–7), the binding energy is considerably less than expected from such a correlation. To explain the activity of the more potent set via a binding mechanism would require binding energies considerably larger than those of the most strongly bound inhibitors.
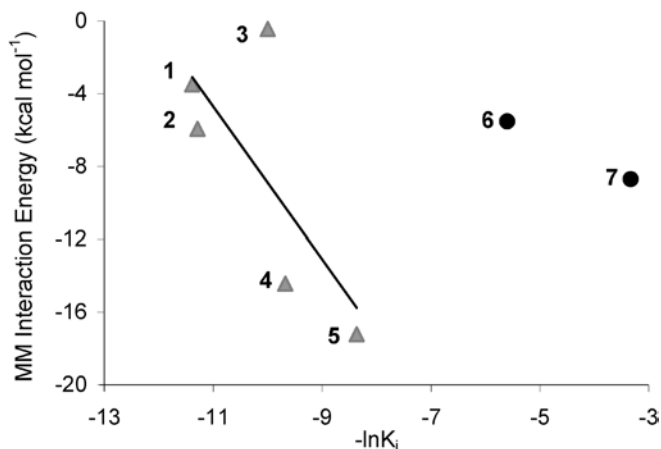
Fig. 9. Plot of relative MM substrate binding energies versus-lnK_i ($r^2 = 0.53$)

Considering the two groups of inhibitors, we can rationalise the QSAR for the more potent set in terms of the σ value. For the less potent inhibitors the actual binding energies, which determine activity, will depend on a combination of factors such as log$P$, steric volume and polarisability.

To investigate whether two groups are predicted at a higher level of theory, these calculations were repeated using the previous MM structures but employing a QM/MM potential. This has the advantage of including the conformational energy of the substrates, which is expected to be less favourable in the enzyme compared to that in aqueous solution, as well as electronic polarisation of the substrate. In the hybrid calculations, the substrate was modelled at the QM(PM3) level, both in the enzyme and in aqueous environments. The MM region was held fixed, and the geometry of each substrate was optimised. The relative binding energies were calculated and plotted as before against −lnK_i (Fig. 10).
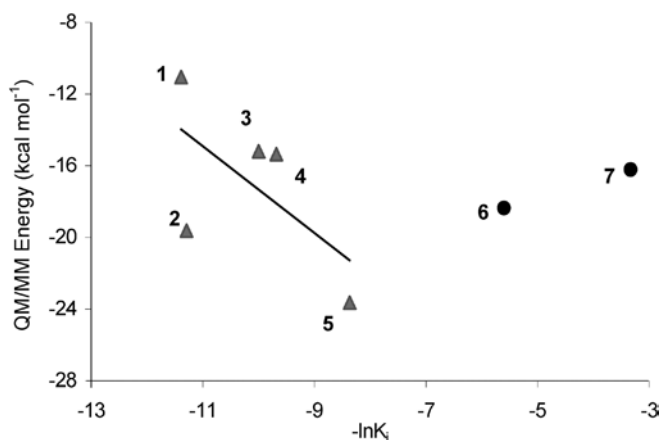
Again the substrates fall into the same two classes, showing that such a division is not dependent on the exact form of the interaction potential used.

Our preliminary calculations thus suggest that these two groups of molecules do inhibit by differing mechanisms and it is plausible to suggest that the more potent set reacts more readily to yield a tetrahedral intermediate whilst the less potent set essentially remains as a Michaelis complex. To test this approximation we are currently carrying out QM/MM calculations of the potential-energy profile leading to the tetrahedral intermediate for a similar range of inhibitors. Initial results show that compared to the less potent set, those in the more potent set have distinctly lower barriers and more stable tetrahedral intermediates. This will increase the rate of reaction compared to the less potent set, which reinforces the suggestion of the binding studies that there are indeed two distinct mechanisms of inhibition. The QM/MM calculations also suggest that such a reaction might proceed as a stepwise rather than a concerted process, with serine deprotonation occurring first, followed by nucleophilic attack of the substrate. These results are in agreement with recent work on the corresponding reactions in aqueous solution [43].

Conclusions

We have shown that QM/MM methods can now be used to probe aspects of enzyme catalysis important from both a fundamental and a practical aspect. We have shown, as have others [6], that given suitable parameterisation of the QM/MM potential the KIEs associated with hydride transfer in LADH can be accurately reproduced. We have also shown that QM/MM calculations may have an important role to play in drug discovery, particularly when actual chemical reactions of the inhibitor take place.

Fig. 10. Plot of relative PM3 QM/MM substrate binding energies versus-lnK_i ($r^2 = 0.40$)

References

1. Warshell A, Levitt M (1976) J Mol Biol 103:227
2. Singh UC, Kollman PA (1986) J Comput Chem 7:718
3. Field MJ, Bash PA, Karplus M (1990) J Comput Chem 11:700
4. Hillier IH (1999) J Mol Struct (THEOCHEM) 463:45
5. Hall RJ, Hindle SA, Burton NA, Hillier IH (2000) J Comput Chem 21:1433
6. Alhambra C, Corchado JC, Sanchez ML, Gao J, Truhlar DG (2000) J Am Chem Soc 122:8197
7. Nicoll RM, Hindle SA, MacKenzie G, Hillier IH, Burton NA (2001) Theor Chem Acc 106:105
8. Cui Q, Karplus M (2001) J Am Chem Soc 123:2284
9. Faulder PF, Tresadern G, Chohan KK, Scrutton NS, Sutcliffe MJ, Hillier IH, Burton NA (2001) J Am Chem Soc 123:8604
10. Truhlar DG, Garrett BC (1980) Acc Chem Res 13:440
11. Truhlar DG, Isaacson AD, Garrett BC (1985) In: Baer M (ed) Theory of chemical reaction dynamics, vol 4. CRC, Boca Raton, pp 65–137

12. Liu YP, Lynch GC, Truong TN, Lu DH, Truhlar DG, Garrett BC (1993) J Am Chem Soc 115:2408
13. Liu YP, Lu DH, Gonzalez-Lafont A, Truhlar DG, Garrett BC (1993) J Am Chem Soc 115:7806
14. Allison TC, Truhlar DG (1998) In: Thompson DL (ed) Modern methods for multidimensional dynamics computations in chemistry. World Scientific, Singapore, pp 618–712
15. Hu WP, Liu YP, Truhlar DG (1994) J Chem Soc Faraday Trans 90:1715
16. Chuang YY, Truhlar DG (1997) J Phys Chem A 101:3808:101: 8741
17. Frisch MJ, Trucks GW, Schlegel HB, Gill PMW, Johnson BG, Robb MA, Cheeseman JR, Keith T, Petersson GA, Montgomery JA, Raghavachari K, Al-Laham MA, Zakrzewski VG, Ortiz JV, Foresman JB, Cioslowski J, Stefanov BB, Nanayakkara A, Challacombe M, Peng CY, Ayala PY, Chen W, Wong MW, Andres JL, Replogle ES, Gomperts R, Martin RL, Fox DJ, Binkley JS, Defrees DJ, Baker J, Stewart JPP, Head-Gordon M, Gonzalez C, Pople JA (1995) GAUSSIAN 94. Gaussian, Pittsburgh, PA
18. Pearlman DA, Case DA, Caldwell JW, Ross WS, Cheatham TE, Ferguson DM, Seibel GL, Singh UC, Weiner PK, Kollman PA (1995) AMBER 4.1. University of California, San Francisco
19. Colby TD, Bahnson BJ, Chin JK, Klinman JP, Goldstein BM (1998) Biochemistry 37:9295
20. Cornell WD, Cieplak P, Bayly CI, Gould IR, Merz KM, Ferguson DM, Spellmeyer DC, Fox T, Caldwell TW, Kollman PA (1995) J Am Chem Soc 117:5179
21. Ryde U (1995) Proteins Struct Funct Genet 21:40
22. Corchado JC, Chuang Y-Y, Coitino EL, Truhlar DG (1999) GAUSSRATE, version 8.5/P8.5-G94. University of Minnesota, Minneapolis, based on Corchado JC, Chuang Y-Y, Fast PL, Villa J, Hu W-P, Liu Y-P, Lynch GC, Nguyen KA, Jackels CF, Melissas VS, Lynch BJ, Rossi I, Coitino EL, Fernandez-Ramos A, Steckler R, Garrett BC, Isaacson AD, Truhlar DG (2000) POLYRATE, version 8.5. University of Minnesota, Minneapolis, and on Frisch MJ, Trucks GW, Schlegel HB, Gill PMW, Johnson BG, Robb MA, Cheeseman JR, Keith T, Petersson GA, Montgomery JA, Raghavachari K, Al-Laham MA, Zakrzewski VG, Ortiz JV, Foresman JB, Cioslowski J, Stefanov BB, Nanayakkara A, Challacombe M, Peng CY, Ayala PY, Chen W, Wong MW, Andres JL, Replogle ES, Gomperts R, Martin RL, Fox DJ, Binkley JS, Defrees DJ, Baker J, Stewart JPP, Head-Gordon M, Gonzalez C, Pople JA (1995) GAUSSIAN 94. Gaussian, Pittsburgh, PA
23. Page M, McIver JW (1988) J Phys Chem 88:922
24. Lu D-H, Truong TN, Melissas VS, Lynch GC, Liu Y-P, Garrett BC, Steckler R, Isaacson AD, Rai SN, Hancock G, Lauderdale JG, Joseph T, Truhlar DG (1992) Comput Phys Commun 71:235
25. Fernandez-Ramos A, Truhlar DG (2001) J Chem Phys 114:1491
26. Swain CG, Stivers EC, Reuwer JF, Schaad LJ (1958) J Am Chem Soc 80:5885
27. Saunders WH (1985) J Am Chem Soc 107:164
28. Huskey WP (1991) J Phys Org Chem 4:361
29. (a) Bahnson BJ, Park DH, Kim K, Plapp BV, Klinman JP (1993) Biochemistry 32:5503; (b) Bahnson BJ, Klinman JP (1995) Methods Enzymol 249:373
30. (a) Sekhar VC, Plapp BV (1990) Biochemistry 29:4289; (b) Shearer GL, Kim K, Lee KM, Wang CK, Plapp BV (1993) Biochemistry 32:11186
31. Hehre WJ, Radom L, Schleyer PvR, Pople JA (1986) Ab initio molecular orbital theory. Wiley, New York
32. Kim Y, Truhlar DG, Kreevoy MM (1991) J Am Chem Soc 113:7837
33. Basran J, Sutcliffe MJ, Scrutton NS (1999) Biochemistry 38:3218
34. Reddy MR, Erion MD (1998) J Enzyme Inhib 14:1
35. Åqvist J, Medina C, Samuelsson JE (1994) Protein Eng 7:385
36. Bohm HJ (1992) J Comput -Aided Mol Des 6: 593
37. Edwards PD, Wolanin DJ, Andisik DW, Davis MW (1995) J Med Chem 38:76
38. Fersht AR (1999) Structure and mechanism in protein science. Freeman, New York.
39. Taylor PJ, Wait A (1986) J Chem Soc Perkins Trans 2:1765
40. Chan AWE, Golec JMC (1996) Bioorg Med Chem 4:1673
41. Bode W, Meyer E Jr, Powers JC (1989) Biochemistry 28:1951
42. Besler BH, Merz KM, Kollman PA (1990) J Comput Chem 11:431
43. Strajbl M, Florian J, Warshel A (2000) J Am Chem Soc 122:5354